Journal of Electronic Materials (2023) 52:1050–1056
https://doi.org/10.1007/s11664-022-10060-8

ORIGINAL RESEARCH ARTICLE

High-Transmittance $(K_{0.5}Na_{0.5})NbO_3$ Ferroelectric Ceramics Modified by $Sr(Bi_{0.5}Ta_{0.5})O_3$

Liwen Wang[1] · Haonan Liu[1] · Chengjian Yu[1] · Kaishuo Liu[1] · Hua Wang[1,2] · Jiwen Xu[1,2] · Ling Yang[1] · Wei Qiu[1]

Received: 20 June 2022 / Accepted: 27 October 2022 / Published online: 18 November 2022

Abstract
$(1-x)(K_{0.5}Na_{0.5})NbO_3$-$x$$Sr(Bi_{0.5}Ta_{0.5})O_3$ (KNN-xSBT, $x=0.018$, 0.02, 0.022, 0.024, 0.026, 0.028) transparent ferroelectric ceramics were prepared using the solid-phase method. The phase structure, microstructure, light transmittance, and optical and electrical properties of KNN-xSBT were investigated. It was found that the pseudo-cubic phase structure, higher compactness, and smaller grains of KNN can be effectively regulated by introducing the second component, SBT, thus achieving strong light transmittance and good energy storage performance for KNN-xSBT ceramics. When $x=0.022$, the near-infrared band (1100 nm) transmittance of the ceramics reaches 72.2%, with energy storage density (W_{rec}) of 0.53 J/cm^3; the maximum dielectric constant is obtained for ceramics at $x=0.018$, with a value of 2935. The KNN-xSBT ceramic sample has relaxor ferroelectric properties and is an environmentally friendly lead-free transparent ferroelectric ceramic.

Keywords Transparent ceramics · lead-free · ferroelectric ceramics · energy storage

Introduction

Transparent ceramics have been widely used in the field of electronics, energy storage, and some extreme environments due to their better thermal, mechanical and excellent chemical stability.[1,2] As potential candidates for new electronic products, transparent ferroelectric ceramics have promising applications in emerging fields such as solid-state lighting, scintillating applications, composite armors, optical components, electro-optical devices, and even biomedical materials, such as screens, etc.[3,4] To date, lead-based transparent ferroelectric ceramics such as lead lanthanum zirconate titanate (PLZT) have been widely studied and applied; however, the lead is harmful to human health and the environment,[5,6] which necessitates the active development of lead-free ceramic materials to replace lead-based ceramics.[7,8]

Perovskite-type lead-free ceramics such as $(Bi_{0.5}Na_{0.5})TiO_3$ (BNT) and $(K_{0.5}Na_{0.5})NbO_3$ (KNN) have the potential to replace lead-based ceramics.[9] KNN ceramics have a large coupling coefficient, excellent electrical properties, high energy storage performance, and light transmittance in the visible and infrared regions, and have become the most widely studied calcium one of the ferroelectric materials with a titanite crystal structure.[10–12] However, pure KNN ceramics are usually opaque and have low density due to the volatilization of alkali metal ions (such as K^+ and Na^+).[13] The transmittance of ceramics is affected by many factors, including phase structure, grain size, and relative density.[14] According to literature reports, the introduction of divalent ions into the positions A and B of the second component of KNN ceramics can achieve the effect of controlling the grain growth of the ceramics, and can also improve the density and adjust the phase structure.[15–17] Among them, doping of Sr^{2+} ($R=1.44$ Å, CN = 12) can significantly improve the electrical properties of ceramic samples.[18,19] Bi_2O_3 is usually used as a sintering aid, and it has an obvious effect on reducing the sintering temperature of ceramics, which can reduce the grain size and increase the density of ceramics.[20–22] However, the high valence of Bi^{3+} ($R=1.38$ Å, CN = 12) may lead to an increase in the obstacles of the ceramic structure and inhibit the growth of grains.[23] The solid solution of the second component $Sr(Bi_{0.5}Ta_{0.5})O_3$ (SBT) significantly

✉ Hua Wang
wh65@tom.com

[1] School of Materials Science and Engineering, Guilin University of Electronic Technology, Guilin 541004, People's Republic of China

[2] Guangxi Key Laboratory of Information Materials, Guilin University of Electronic Technology, Guilin 541004, People's Republic of China

inhibits the growth of crystal grains, so that the grain size of the ceramic sample reaches the nanoscale, which effectively improves the optical transmittance of the ceramic sample. In addition, the grain size affects the breakdown strength (BDS) of the ceramic, where the smaller the grain size, the higher the BDS, and enhances the energy storage potential of the ceramic sample.[24]

Transparent ceramics typically possess high density, few pores at grain boundaries, cubic phase structure with low anisotropy, lack of impurities, and moderate grain size. Additional attractive properties include fineness of raw powders, high uniformity of granulation, and appropriate sintering temperature. Nevertheless, special sintering techniques such as hot isostatic pressing (HIP), spark plasma sintering (SPS), and hot-pressing (HP) may impose excessive cost and the need for complicated processes.[13] HIP, a technique in which gas-assisted pressure is applied three-dimensionally to the compact, seems to be advantageous for the fabrication of dense ceramics with homogeneous microstructure and desired complex shapes, in comparison with pressureless sintering and uniaxial HP techniques[25]; spark plasma sintering (SPS), while reducing the volatility of obtained samples, is characterized by a rapid heating and consolidation rate. The use of SPS allows for dramatically reduced sintering times. Compared with traditional sintering processes, which take on the order of hours to days to complete, a typical SPS process ranges from tens of minutes to a few hours and provides overall better performance,[4] whereas HP has a higher product yield and greatly enhanced specimen density, and reduced cracking and warping of the plates during the final densification phase.[26] But these processes have higher technological requirements, leading to problems of high cost and complex fabrication. Although it is difficult to obtain KNN-based transparent ceramics with stable composition and high density by solid-phase sintering, it can be used as a new method for the preparation of KNN-based transparent ceramics due to its advantages of simple fabrication and low cost.

In this study, a second component, $Sr(Bi_{0.5}Ta_{0.5})O_3$ (SBT), is introduced into KNN to modify its phase structure, grain size, and relative density, thereby improving its optical and electrical properties.

Experimental Details

$(1-x)(K_{0.5}Na_{0.5})NbO_3$-$x$$Sr(Bi_{0.5}Ta_{0.5})O_3$ (KNN-xSBT, $x=0.018$, 0.02, 0.022, 0.024, 0.026, 0.028) transparent ferroelectric ceramics were prepared using the solid-phase method. Analytical-grade reagents Na_2CO_3 (99.8%), K_2CO_3 (99.5%), Nb_2O_5 (99.99%), Ta_2O_5 (99.99%), Bi_2O_3 (99.999%), and $SrCO_3$ (99.9%) were used as the raw chemicals, with the error controlled within 0.0005 g, and 99% ethanol solution and zirconium balls were used as the medium. The powder was poured into a ball mill jar, and 50 ml of ethanol solution was added along with two kinds of zirconium balls with diameters of 5 mm and 8 mm in a quantity ratio of 2:1. The powder was subjected to a rolling ball mill at 410 rpm for 24 h, and then dried and sintered at 860°C with a heating rate of 4°C/min. The powder was ball milled a second time and dried, after which 5 wt.% polyvinyl alcohol (PVA) solution was added and the mixture was passed through a 100-mesh sieve. The granulated powders were pressed into a disk with a diameter of 12 mm. Firstly, the PVA in the blanks was eliminated at 600°C for 2 h, followed by sintering at 1180°C for 2 h. The blanks were polished to 0.3 mm to test the optical properties, phase structure, and surface micro-morphology of the samples.

The optical transmittance of the sample was measured in the range of 200–1100 nm using an ultraviolet–visible–infrared (UV–Vis–IR) spectrophotometer (PerkinElmer Lambda 950, Waltham, MA, USA), and the optical bandgap of the sample was calculated. The phase composition of the sintered samples was identified by x-ray diffraction (XRD, D8 Advance, Bruker) with diffraction angles ranging from 20° to 80°. The microstructures of the sample surface were characterized using field emission scanning electron microscopy (FE-SEM, Quanta 450 FEG, FEI), and the average grain size of the sample was calculated. Silver paste was fired on both sides of the samples at 600°C for 1 h as the electrodes for the dielectric and piezoelectric measurements. The samples were placed in a silicon oil bath for polarization by applying 30–200 kV to test for their electrical hysteresis lines by a ferroelectric integrated system (P-PMF, Radiant Technologies) at room temperature.

Results and Discussion

The transmission spectra of the KNN-xSBT ceramic samples tested in the range of 200–1100 nm and the physical image of the ceramic samples are shown in Fig. 1. In Fig. 1a, all KNN-xSBT samples have a certain light transmittance. For the KNN-xSBT samples with $x=0.022$ and $x=0.024$, it can be seen that the letters below the ceramic are very clear, indicating that these two samples have higher transmittance than other samples, which is also confirmed by test results for light transmittance shown in Fig. 1b and c. Here, it can be seen that the transmittance of the KNN-xSBT ceramic samples first increases and then decreases with the increase in the second component SBT. When $x=0.022$, the transmittance of the KNN-xSBT ceramics reaches the highest transmittance of 69.36% in the visible light band (780 nm) and 72.2% in the near-infrared band. At the same temperature, the transparent ceramics with the same composition

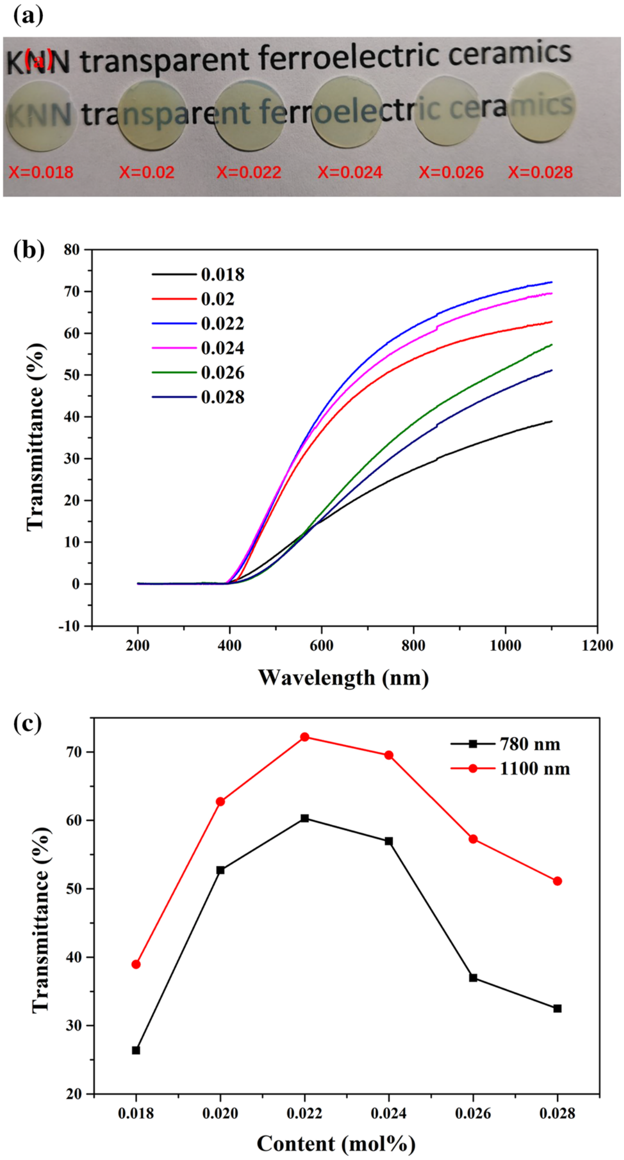

Fig. 1 (a) Photograph of the KNN-*x*SBT transparent ceramics. (b) and (c) The variation curves of transmittance (%) with wavelength (nm) in the range of 200–1100 nm and content (*x*), respectively.

are subjected to other treatments and then applied pressure is the most effective practice to improve transmittance presently, the transmittance of the ceramics at 1100 nm reached the highest 78.5%, while the transmittance of the ceramic samples without pressure is 70.2%, which is a significant difference.[26]

Figure 2a shows the diffraction patterns of the KNN-SBT in the range of 20°–80°. Compared with the KNN standard card (PDF#77-1133), with the increase in the content of SBT, the diffraction peaks show obvious changes. From $x=0.018$ to $x=0.028$, the XRD pattern of the ceramic samples shows no impurity peaks, and the intensity changes in the diffraction peaks are weak, indicating that the ceramic

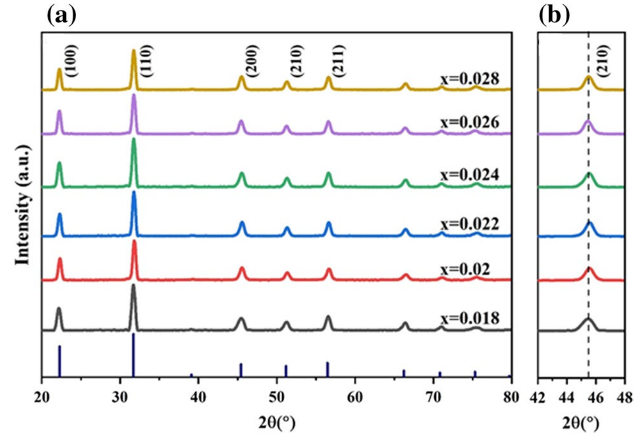

Fig. 2 (a) XRD pattern of KNN-*x*SBT ceramics; (b) magnified XRD pattern in the 2θ range at 42°–48°.

samples have the standard perovskite structure and that the second component SBT is completely integrated into the KNN unit cell to form a homogeneous solid solution without generating a second phase. To further analyze the effect of SBT on the phase structure, the (200) diffraction peak of XRD in the range of 42°–48° is magnified. Figure 2b shows that there is no splitting of the diffraction peaks, which indicates that the introduction of the second component SBT has successfully regulated the phase structure of KNN ceramics, resulting in a phase structure transformation from tetragonal to pseudo-cubic phase. With the increase in SBT, the diffraction peak angle shifts from high to low, which is because of the substitution between ions with different radii and the outermost electrons in the system. When the Bi^{3+} ($R=1.38$ Å, CN = 12) and Ta^{5+} ($R=0.64$ Å, CN = 6) replace Nb^{5+} (0.64 Å, CN = 6) of the B-position in the KNN unit cell, oxygen vacancies will be generated in the unit cell to achieve valence balance, and as the amounts of Bi^{3+} ($R=1.38$ Å, CN = 12) and Ta^{5+} ($R=0.64$ Å, CN = 6) increase, more oxygen vacancies will be generated in the unit cell. Eventually, the unit cell structure collapses, which causes lattice distortion, thus leading to smaller cell volume and a shift of the (200) diffraction peak to a higher angle. In addition, the ionic radius of Sr^{2+} ($R=1.44$ Å, CN = 12) is smaller than that of K^{+} ($R=1.64$ Å, CN = 12) and larger than that of Na^{+} ($R=1.39$ Å, CN = 12). Therefore, the ionic radii of Sr^{2+} and Na^{+} are closer, so it is easier for Sr^{2+} to replace Na^{+}, resulting in an increase in the unit cell volume.[27-29]

The unit cell parameters were calculated based on the XRD data using JADE 6.0 software and are listed in Table I. With the increase in SBT doping content, the a, b, and c of all ceramic samples are very close, and the value of c/a is close to 1, which indicates that the crystal structure of all ceramic samples is in a pseudo-cubic phase structure. Abnormal diffraction peaks appear at $0.02 \leq x \leq 0.024$ and shift to higher angles, which may also be caused by changes in the phase structure. Due to the optical isotropy of the highly symmetric cubic phase, only one refractive index n_0 is given for the incident light that passes through the ceramic sample, and no new scattering center is generated at the grain boundary, thereby reducing the scattering of the incident light, which can significantly improve the optical transmittance of the ceramic sample. For this reason, KNN-*x*SBT ceramics have excellent light transmittance.[27,28]

The addition of the second component SBT significantly inhibits the growth of KNN-based ceramic grains during the ceramic sintering process, so that the grain size of KNN-*x*SBT ceramics reaches the nanoscale, which effectively improves its transmittance to incident light. The microstructure of the KNN-*x*SBT ceramic sample at ×30,000 magnification is shown in Fig. 3. It can be seen that the KNN-*x*SBT ceramics have fine grains and a dense microstructure. In Fig. 3a and e, when $x = 0.018$ and $x = 0.026$, the surface grains of the ceramic samples are slightly melted, the grain boundaries are blurred, and the grains are irregular in shape, which is probably due to the high sintering temperature. The high light transmittance of KNN-*x*SBT ceramics is derived from the symmetrical pseudo-cubic phase structure and the dense microstructure of the KNN-*x*SBT ceramics, which are confirmed by the XRD patterns in Fig. 2 and by the SEM morphology in Fig. 3. However, when comparing the properties of these two series of ceramics with conventional sintering (CS) and HP sintering, all HP specimens are without obvious pores and have much higher density than the values for CS specimens obtained by SEM as reported in the literature,[30] which is also evidence that HP samples have better light transmittance.[31,32]

Table I The lattice parameters of KNN-*x*SBT ceramics

x	*a* (Å)	*b* (Å)	*c* (Å)	*V* (Å^3)	*c/a*
0.018	3.9689	3.9826	3.9922	63.10	1.0059
0.02	3.9830	3.9764	3.9741	62.94	0.9978
0.022	3.9674	3.9825	3.9840	62.95	1.0004
0.024	3.9808	3.9822	3.9787	63.07	0.9995
0.026	3.9870	3.9828	3.9728	63.09	0.9964
0.028	3.9818	3.9818	3.9832	63.15	1.0042

Figure 4 shows the *P*–*E* hysteresis loops of the KNN-*x*SBT ceramics at room temperature under an applied electric field of 80 kV. It can be seen that all the KNN-*x*SBT ceramics have saturated hysteresis loops, and the hysteresis loops become thinner with the increase in the content of SBT. The temperature-dependent dielectric constant (ε_r) and loss (tanδ) of the KNN-*x*SBT ceramics at 1 kHz, 10 kHz, and 100 kHz test frequencies are shown in Fig. 5, where the double peaks merge into a broad peak with increasing SBT from low to high temperature in the ceramics, which is considered as evidence for the transition from ferroelectrics to relaxor ferroelectrics.[28] This indicates that the relaxivity of the KNN-*x*SBT ceramic samples is enhanced, and the introduction of the second component SBT enhanced the symmetry of the phase structure of the KNN-*x*SBT, resulting in a transformation of the phase structure into the pseudo-cubic phase. However, the pseudo-cubic phase structure with higher symmetry makes

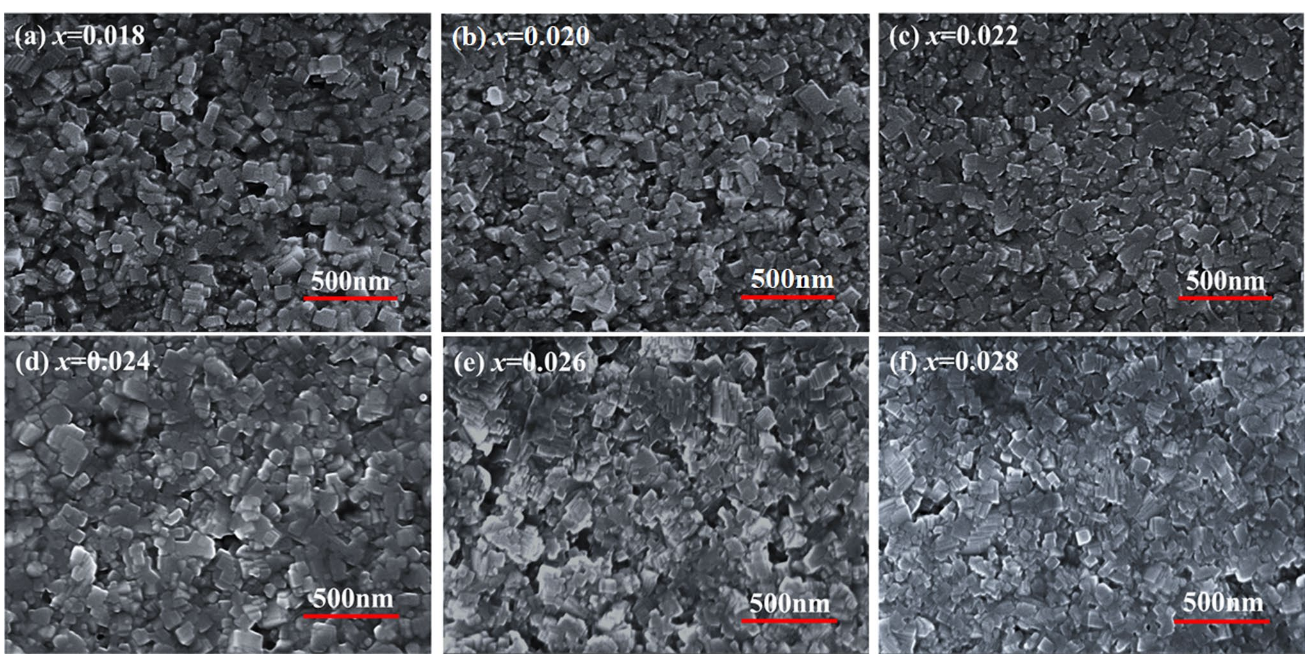

Fig. 3 (a–f) Surface micromorphology and grain size distribution of KNN-*x*SBT ceramics ($x = 0.018$, 0.02, 0.022, 0.024, 0.026, 0.028).

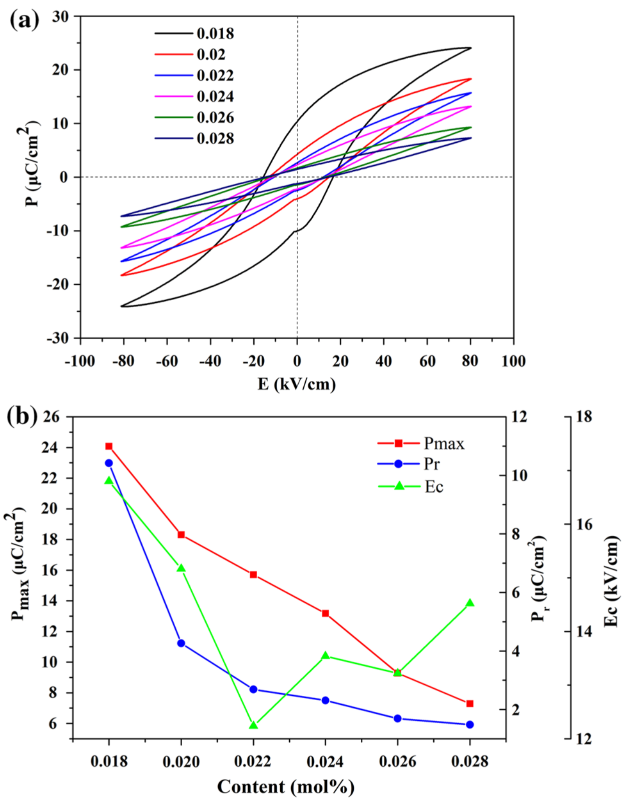

Fig. 4 KNN-xSBT ceramics under 80 kV/cm electric field: (a) P–E hysteresis loops and (b) variation trends of P_m, P_r with content (x).

polarization difficult, and the ferroelectric properties weaken with the increase in SBT.[33] The dielectric constants of the HP specimens are slightly higher than those of the CS samples, the shape of the hysteresis loops for the HP specimens is closer to a square loop than for CS specimens, and the HP specimens more easily reach saturation polarization than the CS specimens.[30] With the increase in the second component, SBT, P_{max} decreases from 24.08 μC/cm^2 when $x=0.018$ to 7.29 μC/cm^2 when $x=0.028$, and P_r decreases from 10.42 μC/cm^2 at $x=0.018$ to 1.48 μC/cm^2 at $x=0.028$, as shown in Fig. 4b. E_c decreases with increasing SBT, from 16.8 kV/cm when $x=0.018$ to 14.52 kV/cm when $x=0.028$. The reason for the gradual weakening of the ferroelectric properties of the KNN-xSBT ceramic samples is closely related to the change in the phase structure. By comparison with values from the corresponding references, for the same ceramic samples, high P_r and low E_c values are obtained by hot pressing relative to pressureless sintering.[30] The energy storage density W of ferroelectric ceramics can be estimated according to its P–E hysteresis loop using Eq. 1:

$$W = \int_0^{P_{max}} E\mathrm{d}P \tag{1}$$

where E is the electric field and P is the polarization. The recoverable energy storage density W_{rec} can be calculated according to the following Eq. 2:

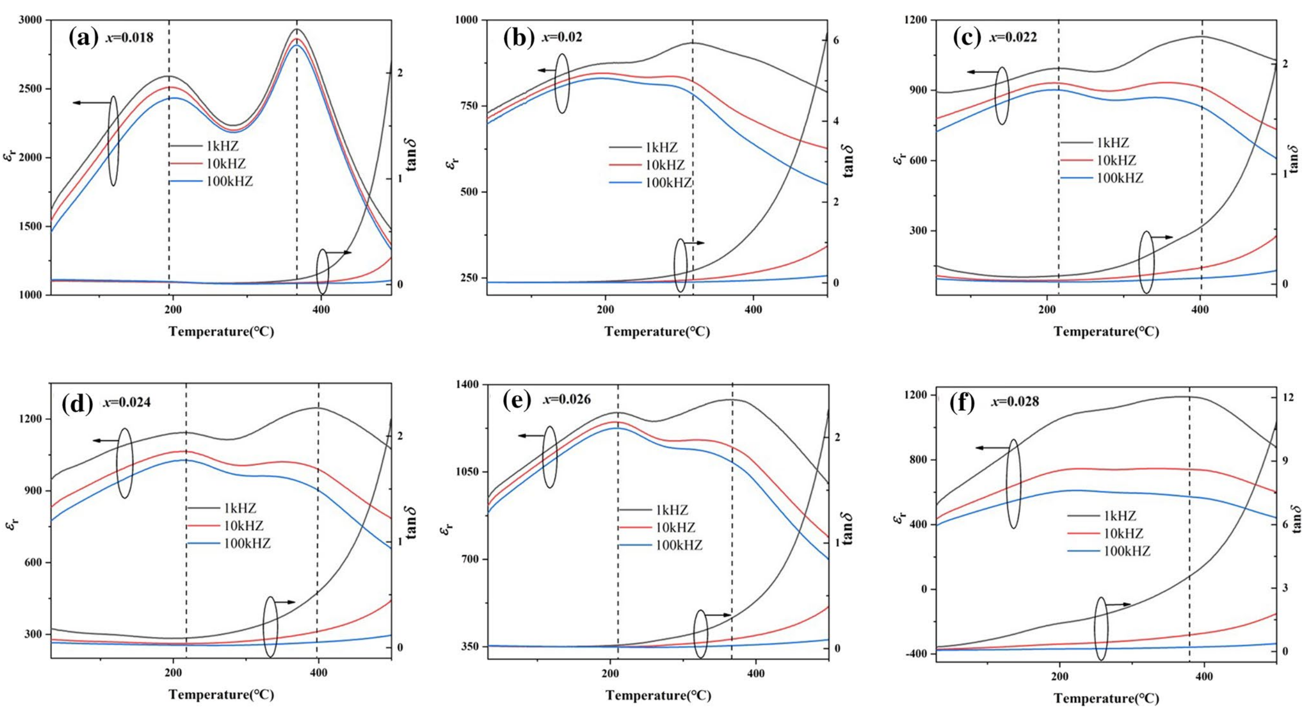

Fig. 5 Temperature-dependent dielectric constant (ε_r) and loss (tanδ) of the KNN-xSBT ceramics.

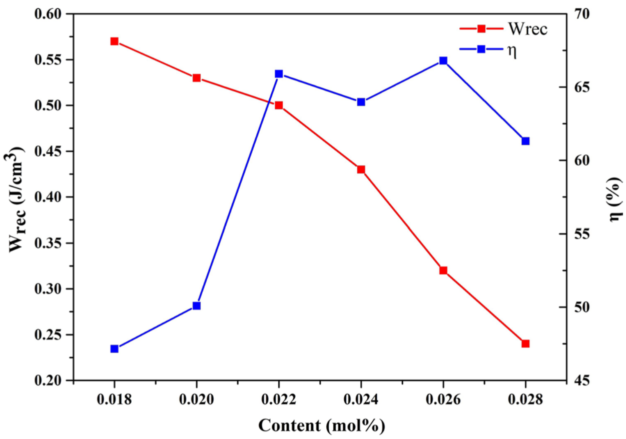

Fig. 6 Variation trends of W_{rec} and η with content (x).

$$W_{rec} = \int_{P_r}^{P_{max}} E\mathrm{d}P \tag{2}$$

Energy storage efficiency η is also an important parameter for measuring the energy storage performance of materials, and energy storage efficiency η can be calculated by Eq. 3:

$$\eta = \frac{W_{rec}}{W} = \frac{W_{rec}}{W_{rec} + W_{loss}} \times 100\% \tag{3}$$

According to the above equations, using the P–E hysteresis loop of the KNN-SBT ceramic samples, the W and W_{rec} of the KNN-SBT ceramic samples are calculated under the critical breakdown strength. The energy storage performance of ceramic samples with different SBT doping content was studied.[27]

According to the P–E hysteresis loop of KNN-xSBT ceramics, its recoverable W_{rec} and energy storage efficiency η were calculated as shown in Fig. 6. The recoverable W_{rec} of KNN-xSBT is up to 0.57 J/cm^3 when the second component $x = 0.018$, and then decreases as x increases. W_{rec} decreases to 0.24 J/cm^3 with $x = 0.028$, and the η of KNN-SBT ceramics reaches the highest value of 66.8% when $x = 0.026$. The best overall energy storage performance of the KNN-xSBT ceramics is achieved with values of $W_{rec} = 0.53$ J/cm^3 and $\eta = 50.09\%$ when $x = 0.022$.

Conclusions

KNN-xSBT transparent ferroelectric ceramics can be successfully prepared using the solid-phase method. The introduction of a second component, SBT, significantly affects the phase structure and microstructure of KNN ceramics, thereby affecting their light transmittance, ferroelectric relaxation behavior, and energy storage characteristics. When $x = 0.022$, the maximum transmittance of 69.36% and 72.2% is reached in the bands at 780 nm and 1100 nm, respectively. It can be seen that the P–E loop changes from the typical P–E loops of ferroelectrics to slim loops, and the curves in the dielectric thermogram merge from double peaks into one broad peak with the increase in the SBT content, which illustrates the transition to relaxor ferroelectrics. As a result, the ferroelectric properties are decreased and the energy storage performance is improved. When $x = 0.022$, the KNN-SBT ceramics have the best comprehensive energy storage performance: $P_{max} = 15.7$ μC/cm^2, $P_r = 2.69$ μC/cm^2, $E_c = 12.24$ kV/cm, $W_{rec} = 0.53$ J/cm^3, $\eta = 50.09\%$. The W_{rec} decreases with the increase in x, and the energy storage efficiency of all the KNN-xSBT ceramics is greater than 45%. The results show that the $0.978(K_{0.5}Na_{0.5})NbO_3$-$0.022Sr(Bi_{0.5}Ta_{0.5})O_3$ is a potential ferroelectric multifunctional material with excellent transmittance and good energy storage properties.

Acknowledgments This work is supported by the National Natural Science Foundation of China (61965007), Guangxi Natural Science Foundation, P. R. China (2018GXNSFDA281042), and Guangxi Key Laboratory of Information Materials (Guilin University of Electronic Technology), P. R. China (201007-Z).

Conflict of interest The authors declare no competing financial interests.

References

1. S.F. Wang, J. Zhang, D.W. Luo, F. Gu, D.Y. Tang, Z.L. Dong, G.E.B. Tan, W.X. Que, T.S. Zhang, S. Li, and L.B. Kong, Transparent ceramics: processing, materials and applications. *Prog. Solid State Chem.* 41, 20 (2013).
2. H.T. Wu, G.B. Hu, S.Y. Shi, X. Liu, H. Wang, J.W. Xu, L. Yang, W. Qiu, and S.J. Zhou, Effect of Ho addition on the optical and electrical properties of 0.98KNN-0.02SYT ceramics. *J. Electron. Mater.* 51, 831 (2022).
3. Z.H. Xiao, S.J. Yu, Y.M. Li, S.C. Ruan, L.B. Kong, Q. Huang, Z.R. Huang, K. Zhou, H.B. Su, Z.J. Yao, W.X. Que, Y. Liu, T.S. Zhang, J. Wang, P. Liu, D.Y. Shen, A. Mathieu, J. Zhang, and D.Y. Tang, Materials development and potential applications of transparent ceramics: a review. *Mater. Sci. Eng. R Rep.* 139, 100518 (2020).
4. X.Q. Chen and Y.Q. Wu, Fabrication and optical properties of highly transparent MgO ceramics by spark plasma sintering. *Scr. Mater.* 162, 14 (2019).
5. P.K. Panda, Review: environmental friendly lead-free piezoelectric materials. *J. Mater. Sci.* 44, 5049 (2009).
6. G.H. Haertling, Ferroelectric ceramics: history and technology. *J. Am. Ceram. Soc.* 82, 797 (1999).
7. S.F. Wang, Q.B. Liu, E.P. Cai, F.H. Mou, and A. Xue, Relaxor behavior and superior ferroelectricity of Y_2O_3-doped $(Ba_{0.98}Ca_{0.02})(Ti_{0.94}Sn_{0.04}Zr_{0.02})O_3$ lead-free ceramics. *J. Rare Earths.* 40, 942 (2022).
8. Y.B. Sun, H. Wang, G.B. Liu, H. Xie, C.R. Zhou, G.H. Chen, C.L. Yuan, and J.W. Xu, High energy storage efficiency and high

electrostrictive coefficients in BNT-BS-*x*BT ferroelectric ceramics. *J. Mater. Sci. Mater. Electron.* 31, 5546 (2020).
9. X.Z. Wang, Y. Huan, Z.X. Wang, X.J. Lin, S.F. Huang, T. Wei, L.T. Li, and X.H. Wang, Electrical conduction and dielectric relaxation mechanisms in the KNN-based ceramics. *J. Appl. Phys.* 126, 104101 (2019).
10. B. Chen, P.F. Liang, D. Wu, X.M. Zhao, X.S. Qiao, Z.H. Peng, L.L. Wei, X.L. Chao, and Z.P. Yang, High-efficiency synthesis of high-performance $K_{0.5}Na_{0.5}NbO_3$ ceramics. *Powder Technol.* 346, 248 (2019).
11. X.M. Zhao, X.L. Chao, D. Wu, P.F. Liang, and Z.P. Yang, Simultaneous realization of high transparency and piezoelectricity in low symmetry KNN-based ceramics. *J. Am. Ceram. Soc.* 102, 3498 (2019).
12. S.T. Li, Y. Yue, X.J. Ning, M. Guo, and M. Zhang, Hydrothermal synthesis and characterization of $(1-x)K_{0.5}Na_{0.5}NbO_3$-$xBi_{0.5}Na_{0.5}TiO_3$ lead-free ceramics. *J. Alloys Compd.* 586, 248 (2014).
13. C. Lin, H.J. Wang, J.Z. Ma, B.Y. Deng, W. Xiao, T.F. Lin, X.H. Zheng, and Y. Xing, Effect of dwell time on cold sintering assisted sintering based highly transparent $0.9K_{0.5}Na_{0.5}NbO_3$–$0.1LiBiO_3$ ceramics. *J. Alloys Compd.* 826, 154249 (2020).
14. Z.Y. Cen, X.H. Wang, Y. Huan, Y.C. Zhen, W. Feng, and L.T. Li, Defect engineering on phase structure and temperature stability of KNN-based ceramics sintered in different atmospheres. *J. Am. Ceram. Soc.* 101, 3032 (2018).
15. B.Y. Qu, H.L. Du, Z.T. Yang, and Q.H. Liu, Large recoverable energy storage density and low sintering temperature in potassium-sodium niobate-based ceramics for multilayer pulsed power capacitors. *J. Am. Ceram. Soc.* 100, 1517 (2017).
16. G.B. Hu, H.N. Liu, J.T. Wang, Y.B. Sun, H. Wang, J.W. Xu, and L. Yang, Regulating the structural, transmittance, ferroelectric, and energy storage properties of $K_{0.5}Na_{0.5}NbO_3$ ceramics using $Sr(Yb_{0.5}Nb_{0.5})O_3$. *J. Electron. Mater.* 50, 968 (2021).
17. G.B. Hu, J.T. Wang, X. Liu, H.N. Liu, H. Wang, J.W. Xu, L. Yang, C.R. Zhou, and W. Qiu, Structural, transmittance, ferroelectric, energy storage, and electrical properties of $K_{0.5}Na_{0.5}NbO_3$ ceramics regulated by $Sr(Yb_{0.5}Ta_{0.5})O_3$. *J Mater. Sci. Mater. Electron.* 32, 22300 (2021).
18. J. Jumpatam, B. Putasaeng, N. Chanlek, and P. Thongbai, Influences of Sr^{2+} doping on microstructure, giant dielectric behavior, and non-ohmic properties of $CaCu_3Ti_4O_{12}/CaTiO_3$ ceramic composites. *Molecules* 26, 1994 (2021).
19. J. Jumpatam, B. Putasaeng, N. Chanlek, J. Boonlakhorn, P. Thongbaid, N. Phromviyo, and P. Chindaprasirt, Significantly improving the giant dielectric properties of $CaCu_3Ti_4O_{12}$ ceramics by co-doping with Sr^{2+} and F-ions. *Mater. Res. Bull.* 133, 111043 (2021).
20. Y.R. Wang, Y.P. Pu, Y.F. Cui, Y. Shi, and H.Y. Zheng, Enhanced energy storage density of $Ba_{0.4}Sr_{0.6}TiO_3$ ceramics with additive of Bi_2O_3-B_2O_3-ZnO glass. *Mater Lett.* 201, 203 (2017).
21. J.Q. Li, J.J. Wang, F.M. Wu, H. Ma, T.Y. Ma, Y. Tian, D.Q. Liu, and B. Yang, Microstructure and electric properties of Bi_2O_3-doped $(K_{0.5}Na_{0.5})NbO_3$ lead-free ceramics. *Coatings.* 12, 526 (2022).
22. X.X. Wang, X.G. Tang, K.W. Kwok, H.L.W. Chan, and C.L. Choy, Effect of excess Bi_2O_3 on the electrical properties and microstructure of $(Bi_{1/2}Na_{1/2})TiO_3$ ceramics. *Appl. Phys. A: Mater. Sci. Process.* 80, 1071 (2005).
23. H.R. Liu, Q. Li, J. Ma, and X.C. Chu, Effects of Bi^{3+} content and grain size on electrical properties of $SrBi_2Ta_2O_9$ ceramic. *Mater. Lett.* 76, 21 (2012).
24. B.B. Liu, X.H. Wang, R.X. Zhang, and L.T. Li, Grain size effect and microstructure influence on the energy storage properties of fine-grained $BaTiO_3$-based ceramics. *J. Am. Ceram. Soc.* 100, 3599 (2017).
25. K. Itatani, T. Tsujimoto, and A. Kishimoto, Thermal and optical properties of transparent magnesium oxide ceramics fabricated by post hot-isostatic pressing. *J. Eur. Ceram. Soc.* 26, 639 (2006).
26. L. Esposito, A. Piancastelli, and S. Martelli, Production and characterization of transparent $MgAl_2O_4$ prepared by hot pressing. *J. Eur. Ceram. Soc.* 33, 737 (2013).
27. H.N. Liu, J.T. Wang, H. Wang, J.W. Xu, C.R. Zhou, and W. Qiu, Er^{3+} and $Sr(Bi_{0.5}Nb_{0.5})O_3$-modified $(K_{0.5}Na_{0.5})NbO_3$: a new transparent fluorescent ferroelectric ceramic with high light transmittance and good luminescence performance. *Ceram Int.* 48, 4230 (2022).
28. J. Zhang, J.W. Xu, L. Yang, Z.J. Cao, C.L. Yuan, C.R. Zhou, H. Wang, and G.H. Rao, Controlling light-induced dielectric response of Sr/Ni-modified $(K_{0.5}Na_{0.5})NbO_3$ ceramics by narrow bandgap method. *Mater. Sci. Semicond Process.* 143, 106521 (2022).
29. H.T. Wu, S.Y. Shi, X. Liu, H. Wang, J.W. Xu, L. Yang, W. Qiu, and S.J. Zhou, The $Ba(Bi_{0.5}Ta_{0.5})O_3$ modified $(K_{0.5}Na_{0.5})NbO_3$ lead-free transparent ferroelectric ceramics with high transmittance and excellent energy storage performance. *J. Mater. Sci. Mater. Electron.* 33, 16045 (2022).
30. G.C. Deng, A.L. Ding, X.S. Zheng, X. Zeng, and Q.R. Yin, Property improvement of $0.3Pb(Zn_{1/3}Nb_{2/3})O_3$–$0.7Pb_{0.96}La_{0.04}(Zr_xTi_{1-x})_{0.99}O_3$ ceramics by hot-pressing. *J. Eur. Ceram. Soc.* 26, 2349 (2006).
31. J.F. Lin, Y. Zhou, Q.L. Lu, X. Wu, C. Lin, T.F. Lin, K.H. Xue, X.S. Miao, B.S. Sa, and Z.M. Sun, Reversible modulation of photoenergy in Sm-doped $(K_{0.5}Na_{0.5})NbO_3$ transparent ceramics via photochromic behavior. *J. Mater. Chem. A.* 7, 19374 (2019).
32. X. Wu, S.B. Lu, and K.W. Kwok, Photoluminescence, electro-optic response and piezoelectric properties in pressureless-sintered Er-doped KNN-based transparent ceramics. *J. Alloys Compd.* 695, 3573 (2017).
33. G.W. Yan, and Q.Q. Qiu, B.J. Fang, Z.H. Chen Correlation between phase structure and polarization of Mg doped $(Ba_{0.98}Li_{0.02})TiO_3$ energy storage ceramics. *J. Mater. Sci: Mater. Electron.* 33, 20981 (2022).